Sensors and Materials, Vol. 35, No. 2 (2023) 521–528
MYU Tokyo

S & M 3190

Development of Ce-doped $Gd_3Al_{5-y}Ga_yO_{12}$ Nanoparticle Scintillators

Masanori Koshimizu,[1*] Yutaka Fujimoto,[2] and Keisuke Asai[2]

[1]Research Institute of Electronics, Shizuoka University, 3-5-1 Johoku, Naka-ku, Hamamatsu 432-8011, Japan
[2]Department of Applied Chemistry, Tohoku University, 6-6-07 Aoba, Aramaki, Aoba-ku, Sendai 980-8579, Japan

(Received October 1, 2022; accepted November 30, 2022)

Keywords: scintillator, nanoparticle, sol–gel method

We synthesized Ce-doped $Gd_3Al_{5-y}Ga_yO_{12}$ (GAGG) nanoparticle scintillators for obtaining efficient emission in living bodies upon X-ray irradiation from outside. To obtain a high photoluminescence quantum yield (QY), the chemical composition and synthesis conditions were optimized. The highest QY of 90%, which is higher than that of a commercially available Ce-doped GAGG single-crystal scintillator (87%), was achieved with the composition for Gd:Al:Ga = 3:3:2, a Ce concentration of 0.1 mol% relative to (Gd + Ce), aging at room temperature for 1 d, and a calcination temperature of 1300 °C. The size of the particles was 200–300 nm. A dominant emission band at around 550 nm was observed in the photoluminescence and X-ray-induced radioluminescence spectra and attributed to the 5d–4f transition of Ce^{3+}. The high photoluminescence QY and appropriate size for applications in living bodies indicated that nanoparticle scintillators based on Ce-doped GAGG were successfully developed.

1. Introduction

Scintillators are phosphors that emit UV, visible, or IR photons upon interaction with ionizing radiation. They have been used for radiation detection in combination with photon detectors such as photomultiplier tubes and photodiodes. As sensors of ionizing radiation, the requirements for scintillators are a high scintillation light yield, fast scintillation decay, appropriate emission wavelength, high interaction probability with the ionizing radiation to be detected, and chemical stability. At present, no scintillators fulfill all requirements simultaneously; therefore, a variety of scintillators are commercially available, and a huge number of scintillators have been developed using various compounds. From the viewpoint of constituents, inorganic,[(1)] organic,[(2)] and organic–inorganic hybrid materials[(3,4)] have been used. Inorganic scintillators based on oxides[(5–8)] or halides[(9–11)] generally have high light yields and high interaction probabilities with high-energy photons (X-rays or gamma rays). Organic scintillators have low scintillation light yields and rapid responsiveness.[(12–14)] As organic–inorganic

*Corresponding author: e-mail: koshimizu.masanori@shizuoka.ac.jp
https://doi.org/10.18494/SAM4149

ISSN 0914-4935
https://myukk.org/

hybrid materials, layered perovskite organic–inorganic compounds exhibiting the efficient and fast emission of quantum-confined free excitons have been used as scintillators.[4,15–17] Also, inorganic-nanoparticle-loaded organic scintillators have been developed, as introduced later. Because the requirements for scintillators are different in different applications, a suitable scintillator has been used for each specific application.

Recently, scintillators have also been used inside living bodies to obtain efficient emission upon irradiation from outside. An example is the use of Ce-doped $Gd_3Al_{5-y}Ga_yO_{12}$ (GAGG) microparticles in a mouse to control the behavior of the mouse via X-ray irradiation.[18] To introduce scintillators in living bodies in a less invasive manner, scintillator nanoparticles are preferable.

The usage of nanoparticles in scintillators is divided into two categories: in one category, nanoparticles are included in scintillators (mainly in organic liquid or plastic scintillators) to enhance the interaction probability of the scintillators with high-energy photons[3,19–24] or to include the sample nuclei for neutron experiments.[25–27] The other category is the use of scintillators in the form of nanoparticles. As examples of this usage, X-ray-induced photodynamic therapy has been performed[28] using Pr-doped $Y_3Al_5O_{12}$[29] or CsI(Na)@MgO[30] nanoparticles. To achieve efficient emission inside a living body, the scintillation light yield should be high. Also, if the emission is induced by X-rays from outside the living body, the interaction probability with X-rays should be high.

In this study, we synthesized Ce-doped GAGG nanoparticle scintillators by the sol–gel method. Ce-doped GAGG was chosen owing to its high scintillation light yield and high effective atomic number and density, which result in a high interaction probability with X-rays. Because the scintillation light yield of nanoparticle scintillators (or scintillator powders in general) is difficult to estimate, the synthesis conditions were optimized to achieve the highest photoluminescence quantum yield (QY). The chemical composition, aging duration, and calcination temperature for obtaining the nanoparticles were optimized.

2. Materials and Methods

L(+)-tartaric acid (Guaranteed Reagent, Wako), $Gd(NO_3)_3{\cdot}6H_2O$ (99.99%, Sigma-Aldrich), $Al(NO_3)_3{\cdot}9H_2O$ (99.997%, Sigma-Aldrich), $Ga(NO_3)_3{\cdot}nH_2O$ (99.999%, Kojundo Chemical Laboratory Co. Ltd.), and $Ce(NO_3)_3{\cdot}6H_2O$ (98.0+%, Wako) were used without further purification. Ce-doped GAGG nanoparticles were synthesized by the sol–gel method in accordance with the literature on the synthesis of Ce- and Pr-doped GAGG nanoparticles.[31] L(+)-tartaric acid was dissolved in 25 mL of distilled water to a concentration of 0.6 M. Subsequently, metal nitrates were dissolved in the solution at a stoichiometric ratio ($Gd_{3-3x}Al_{5-y}Ga_yCe_{3x}O_{12}$: x represents the Ce concentration) with a total cation concentration of 0.3 M. The Ga concentration was confirmed by ICP-AES analysis. The solution was stirred at room temperature for 0–3 d in a beaker covered with Al foil for aging, which was followed by aging at 80 °C for 2 h with stirring. Subsequently, the Al foil was removed and the beaker was heated at 120 °C for longer than 12 h to obtain a dry gel that was then ground and calcined at

1100–1500 °C for 6 h to obtain nanoparticles. The parameters in the synthesis were aging duration at room temperature, host composition (Gd:Al:Ga), Ce concentration, and calcination temperature.

The crystalline phase was confirmed from powder X-ray diffraction (XRD) patterns with Cu Kα radiation using a diffractometer (Ultima IV, Rigaku) equipped with an X-ray tube operated at 40 kV and 40 mA. The shapes and sizes of the nanoparticles were observed using a transmission electron microscope (TEM; HD-2700, Hitachi High-Technologies). The photoluminescence QYs were estimated and excitation–emission maps were obtained using an absolute photoluminescence QY spectrometer (Quantaurus-QY, Hamamatsu). X-ray-induced radioluminescence (XRL) spectra of the nanoparticles were obtained at room temperature using an X-ray generator (Rigaku, SA-HFM3) equipped with a Cu target operated at 40 kV and 40 mA. The XRL photons were delivered via an optical fiber to a CCD-based spectrometer (QE Pro, Ocean Insight).

3. Results and Discussion

Figure 1 shows the XRD patterns of the nanoparticles with Gd:Al:Ga = 3:3:2, 3:4:1, and 3:5:0 for verification of the crystalline phases obtained at a high Al content. Most of the diffraction peaks are attributed to the GAGG phase for the nanoparticles with Gd:Al:Ga = 3:3:2, whereas a significant fraction of the diffraction peaks are attributed to the $GdAlO_3$ phase for Gd:Al:Ga = 3:4:1. For 3:5:0, no GAGG phase is observed, and the diffraction peaks are attributed to mixed phases of $GdAlO_3$ and Gd_2O_3. As presented later, a GAGG phase is also observed for Gd:Al:Ga = 3:2:3. Hence, we discuss the properties of nanoparticles with the compositions of Gd:Al:Ga = 3:3:2 and 3:2:3 in the following.

Next, we discuss the influence of the aging duration at room temperature. TEM images of the nanoparticles with Gd:Al:Ga = 3:3:2 synthesized after aging for 0 and 1 d are presented in Fig. 2. Without aging, an interconnected structure of primary nanoparticles is found. In contrast, after aging for 1 d, separated nanoparticles are obtained. In applications as nanoparticles, the interconnected structure is not appropriate. Hence, aging for at least 1 d is necessary. XRD patterns of the nanoparticles with Gd:Al:Ga = 3:2:3 and 3:3:2 synthesized after aging for 0, 1, and 3 d at room temperature are presented in Fig. 3. The intensity of the diffraction peak at around 30.4°, which is attributed to a subphase of β-Ga_2O_3, increases with the aging duration. On the basis of these results, the optimum duration of the aging is 1 d. In the following, we discuss the properties of nanoparticles synthesized after aging for 1 d at room temperature.

The photoluminescence QY of the nanoparticles with Gd:Al:Ga = 3:3:2 calcined at 1100 °C was 56%, which was significantly higher than that (32%) of the nanoparticles with Gd:Al:Ga = 3:2:3. Hence, we discuss the photoluminescence QY of the nanoparticles with Gd:Al:Ga = 3:3:2 in the following. The photoluminescence QY as a function of the Ce concentration relative to (Gd + Ce) and the calcination temperature is shown in Fig. 4. The highest QY of 90% was achieved for the Ce concentration of 0.1 mol% and the calcination temperature of 1300 °C. Hence, the optimum Ce concentration and calcination temperature are 0.1 mol% and 1300 °C, respectively. The QY of 90% was higher than that (87%) of commercially available Ce-doped GAGG single crystal purchased from C&A Corp. The decrease in the QY

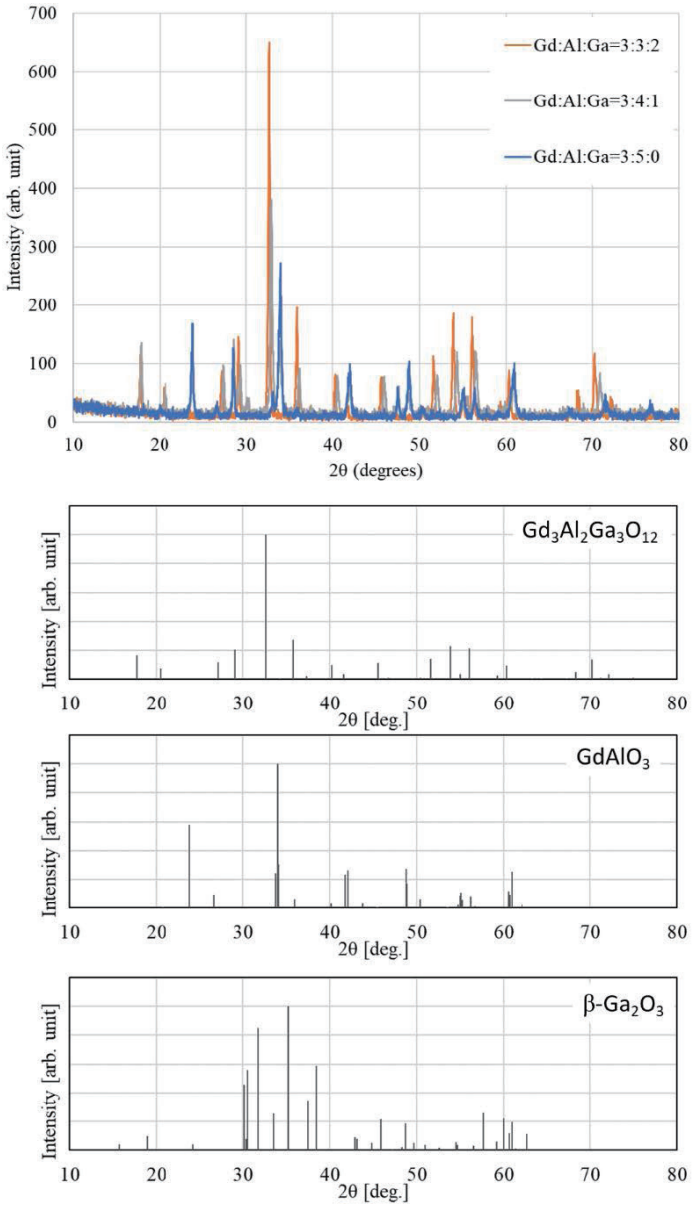

Fig. 1. (Color online) XRD patterns of nanoparticles with Gd:Al:Ga = 3:3:2, 3:4:1, and 3:5:0 with reference patterns.

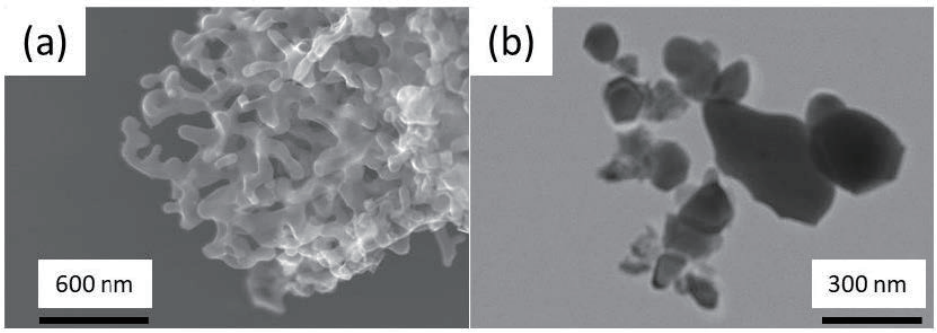

Fig. 2. TEM images of the nanoparticles with Gd:Al:Ga = 3:3:2 synthesized after aging for 0 and 1 d at room temperature.

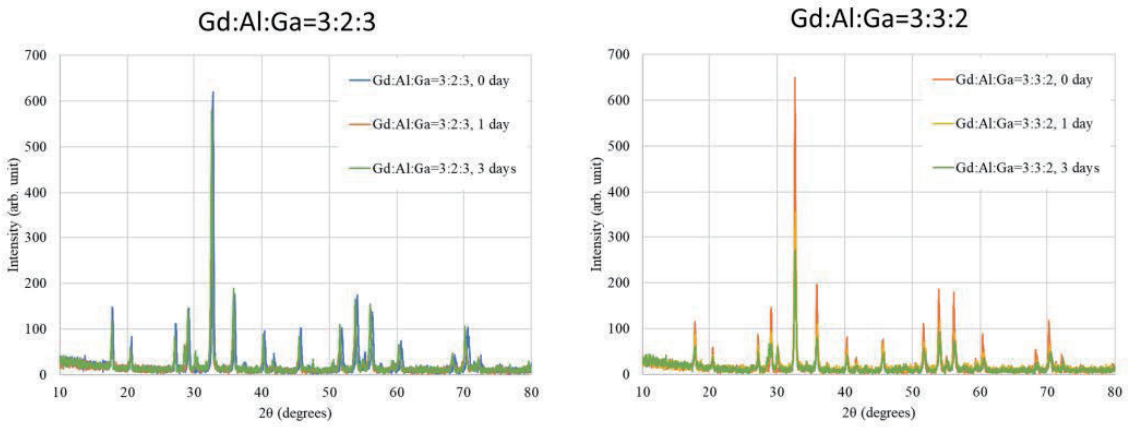

Fig. 3. (Color online) XRD patterns of the nanoparticles with Gd:Al:Ga = 3:2:3 and 3:3:2 synthesized after aging for 0, 1, and 3 d.

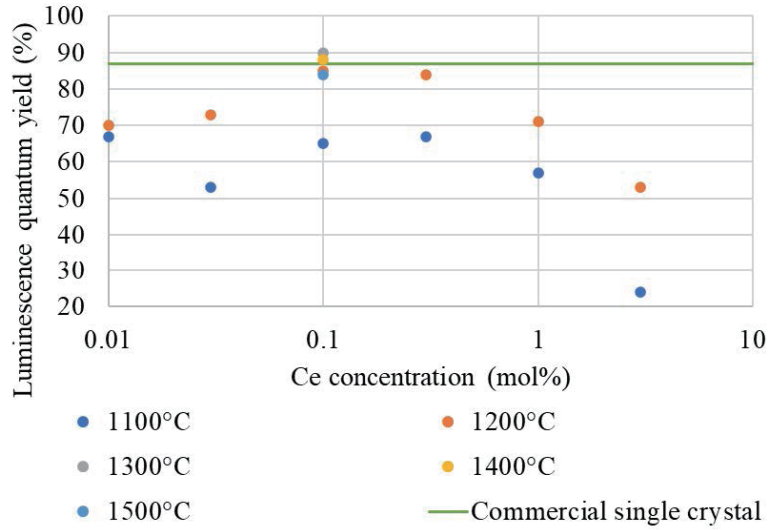

Fig. 4. (Color online) Photoluminescence QY as a function of Ce concentration relative to (Gd + Ce) and calcination temperature.

above 0.3 mol% is attributed to concentration quenching. The increase in the QY up to 1300 °C may be attributed to better crystallinity, while the subsequent decrease may be attributed to the loss of Ga at high temperatures.

Hereafter, we mainly discuss the properties of the nanoparticles synthesized under the optimum conditions for photoluminescence QY. TEM images of the nanoparticles with Gd:Al:Ga = 3:3:2 and a Ce concentration of 0.1 mol% synthesized after aging for 1 d at room temperature and calcined at different temperatures are presented in Fig. 5. The size of the nanoparticles increased with the calcination temperature up to 1300 °C. The size of the nanoparticles calcined at 1300 °C was 200–300 nm, which is suitable for applications in living bodies or biological tissues. A photoluminescence excitation–emission map of the nanoparticles synthesized under the optimum conditions is shown in Fig. 6. Two excitation bands were

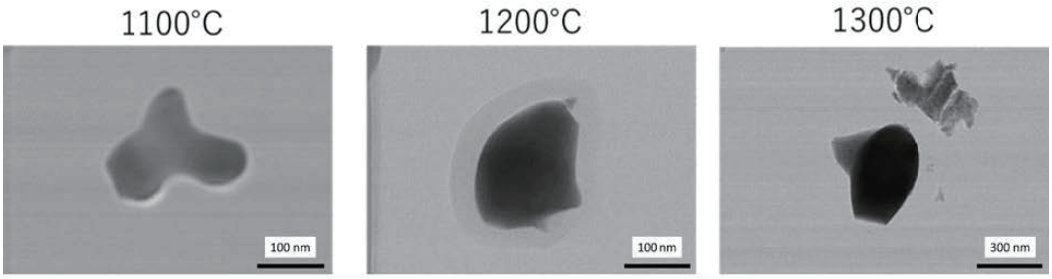

Fig. 5. TEM images of nanoparticles with Gd:Al:Ga = 3:3:2 and Ce concentration of 0.1 mol% synthesized after aging for 1 d and calcined at different temperatures.

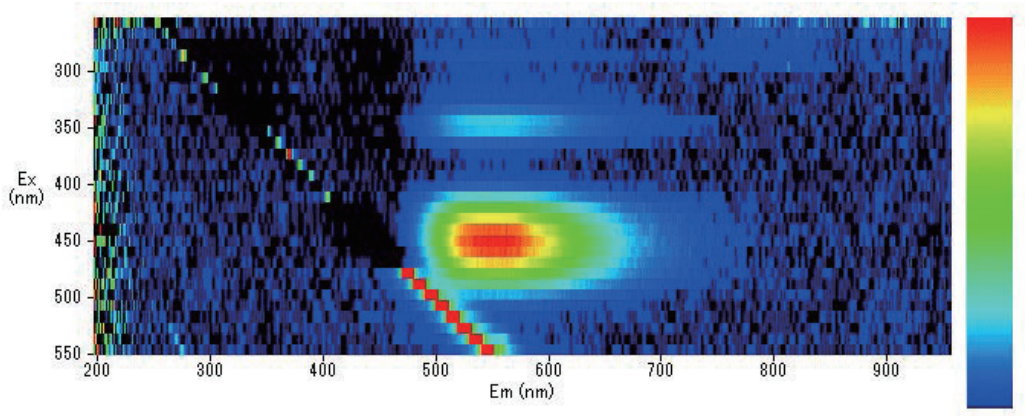

Fig. 6. (Color online) Photoluminescence excitation–emission map of nanoparticles synthesized under the optimum conditions.

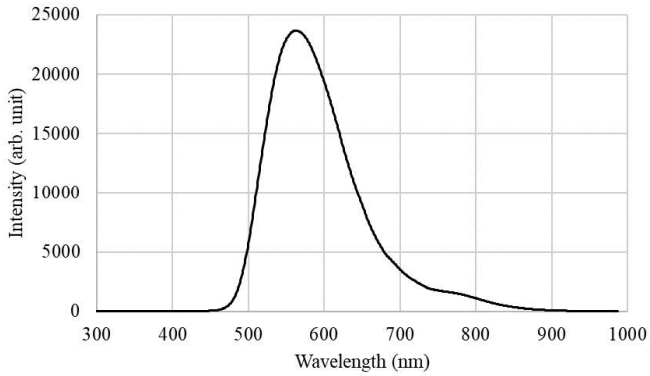

Fig. 7. XRL spectrum of the nanoparticles synthesized under the optimum conditions.

observed at around 350 and 450 nm, which and are attributed to excitations to the $5d_2$ and $5d_1$ levels, respectively. An emission band was observed at 550 nm, which is attributed to the 5d–4f transition. The wavelengths of the bands are consistent with those in a previous paper.[32] The XRL spectrum of the nanoparticles synthesized under the optimum conditions is presented in Fig. 7. An emission band was observed at around 560 nm, which is consistent with that of the photoluminescence emission spectrum. Also, a small shoulder was observed at around 780 nm and may be due to defects in the GAGG host.

4. Conclusions

Ce-doped GAGG nanoparticles were synthesized by the sol–gel method. The optimum conditions for obtaining the highest photoluminescence QY were Gd:Al:Ga = 3:3:2, a Ce concentration of 0.1 mol%, an aging duration of 1 d at room temperature, and a calcination temperature of 1300 °C. The photoluminescence QY reached 90%, which is higher than that of commercially available Ce-doped GAGG single crystal. The size of the nanoparticles increased with the calcination temperature and was 200–300 nm after calcination at 1300 °C. A dominant emission band at around 550 nm was observed in the photoluminescence and XRL spectra. On the basis of these results, the synthesized nanoparticles are judged to be suitable for applications in living bodies or biological tissues in a noninvasive manner with efficient scintillation in the yellow wavelength region.

Acknowledgments

This research was supported by Grants-in-Aid for Scientific Research (A) (No. 22H00308, 2022–2025) and Scientific Research (B) (No. 22H02939, 2022–2024). Part of this research is based on the Cooperative Research Project of the Research Center for Biomedical Engineering, Ministry of Education, Culture, Sports, Science and Technology.

References

1 T. Yanagida: Proc. Japan Academy Ser. B **94** (2018) 75.
2 M. Koshimizu: Jpn. J. Appl. Phys. **62** (2023) 010503. https://doi.org/10.35848/1347-4065/ac94fe
3 M. Koshimizu: Funct. Mater. Lett. **13** (2020) 2030003.
4 N. Kawano, M. Koshimizu, G. Okada, Y. Fujimoto, N. Kawaguchi, T. Yanagida, and K. Asai: Sci. Rep. **7** (2017) 14754.
5 T. Yanagida, T. Kato, D. Nakauchi, and N. Kawaguchi: Sens. Mater. **34** (2022) 595.
6 P. Kantuptim, D. Nakauchi, T. Kato, N. Kawaguchi, and T. Yanagida: Sens. Mater. **34** (2022) 603.
7 D. Nakauchi, H. Fukushima, T. Kato, N. Kawaguchi, and T. Yanagida: Sens. Mater. **34** (2022) 611.
8 P. Kantuptim, H. Fukushima, H. Kimura, D. Nakauchi, T. Kato, M. Koshimizu, N. Kawaguchi, and T. Yanagida: Sens. Mater. **33** (2021) 2195.
9 Y. Fujimoto, D. Nakauchi, T. Yanagida, M. Koshimizu, and K. Asai: Sens. Mater. **34** (2022) 629.
10 Y. Fujimoto, K. Saeki, T. Yanagida, M. Koshimizu, and K. Asai: Radiat. Meas. **106** (2017) 151.
11 Y. Fujimoto, M. Koshimizu, T. Yanagida, G. Okada, K. Saeki, and K. Asai: Jpn. J. Appl. Phys. **55** (2016) 090301.
12 A. Watanabe, A. Magi, M. Koshimizu, A. Sato, Y. Fujimoto, and K. Asai: Sens. Mater. **33** (2021) 2251.
13 A. Magi, M. Koshimizu, Y. Fujimoto, T. Yanagida, and K. Asai: Radiat. Meas. **137** (2020) 106401.
14 A. Sato, M. Koshimizu, Y. Fujimoto, S. Komatsuzaki, S. Kishimoto, and K. Asai: Mater. Chem. Front. **6** (2022) 1470.
15 K. Okazaki, D. Onoda, D. Nakauchi, N. Kawano, H. Fukushima, T. Kato, N. Kawaguchi, and T. Yanagida: Sens. Mater. **34** (2022) 575.
16 D. Onoda, M. Akatsuka, N. Kawano, T. Kato, D. Nakauchi, N. Kawaguchi, and T. Yanagida: Sens. Mater. **34** (2022) 585.
17 N. Kawano, M. Koshimizu, A. Horiai, F. Nishikido, R. Haruki, S. Kishimoto, K. Shibuya, Y. Fujimoto, T. Yanagida, and K. Asai: Jpn. J. Appl. Phys. **55** (2016) 110309.
18 T. Matsubara, T. Yanagida, N. Kawaguchi, T. Nakano, J. Yoshimoto, M. Sezaki, H. Takizawa, S. P. Tsunoda, S. Horigane, S. Ueda, S. Takemoto-Kimura, H. Kandori, A. Yamanaka, and T. Yamashita: Nat. Commun. **12** (2021) 4478.
19 Y. Sun, M. Koshimizu, N. Yahaba, F. Nishikido, S. Kishimoto, R. Haruki, and K. Asai: Appl. Phys. Lett. **104** (2014) 174104.

20 Y. Araya, M. Koshimizu, R. Haruki, F. Nishikido, S. Kishimoto, and K. Asai: Sens. Mater. **27** (2015) 255.
21 F. Hiyama, T. Noguchi, M. Koshimizu, S. Kishimoto, R. Haruki, F. Nishikido, T. Yanagida, Y. Fujimoto, T. Aida, S. Takami, T. Adschiri, and K. Asai: Jpn. J. Appl. Phys. **57** (2018) 012601.
22 F. Hiyama, T. Noguchi, M. Koshimizu, S. Kishimoto, R. Haruki, F. Nishikido, Y. Fujimoto, T. Aida, S. Takami, T. Adschiri, and K. Asai: Jpn. J. Appl. Phys. **57** (2018) 052203.
23 K. Kagami, M. Koshimizu, Y. Fujimoto, S. Kishimoto, R. Haruki, F. Nishikido, and K. Asai: J. Mater. Sci. Electron. **31** (2020) 896.
24 A. Magi, M. Koshimizu, A. Watanabe, A. Yoko, G. Seong, T. Tomai, T. Adschiri, R. Haruki, F. Nishikido, S. Kishimoto, Y. Fujimoto, and K. Asai: J. Mater. Sci. Electron. **32** (2021) 7987.
25 S. Takigawa, M. Koshimizu, T. Noguchi, T. Aida, S. Takami, T. Adschiri, Y. Fujimoto, A. Yoko, G. Seong, T. Tomai, and K. Asai: J. Radioanal. Nucl. Chem. **314** (2017) 611.
26 S. Arai, T. Noguchi, T. Aida, A. Yoko, T. Tomai, T. Adschiri, M. Koshimizu, T. Fujimoto, and K. Asai: J. Ceram. Soc. Jpn. **128** (2019) 28.
27 A. Watanabe, A. Magi, A. Yoko, G. Seong, T. Tomai, T. Adschiri, Y. Hayashi, M. Koshimizu, Y. Fujimoto, and K. Asai: Nanomaterials **11** (2021) 1124.
28 A. Kamkaew, F. Chen, Y. Zhan, R. L. Majewski, and W. Cai: ACS Nano **10** (2016) 3918.
29 A. A. Sapre, E. Novitskaya, V. Vakharia, A. Cota, W. Wrasidlo, S. M. Hanrahan, S. Derenzo, M. T. Makale, and O. A. Graeve: Mater. Lett. **228** (2018) 49.
30 F. Jiang, C. Lee, W. Zhang, W. Jiang, Z. Cao, H. B. Chong, W. Yang, S. Zhan, J. Li, Y. Teng, Z. Li, and J. Xie: J. Nanobiotech. **20** (2022) 330.
31 P. Sengar, K. García-Tapia, B. Can-Uc, K. Juárez-Moreno, O. E. Contreras-López, and G. A. Hirata: J. Appl. Phys. **126** (2019) 083107.
32 T. Yanagida, K. Kamada, Y. Fujimoto, H., Yagi, and T. Yanagitani: Opt. Mater. **35** (2013) 2480.